Bulletin 93

Penetration and Mixing of Heated Discharges into Waterways

J. A. Sehetz
C. H. Lewis
B. L. Sill
J. C. Chien
D. Markham

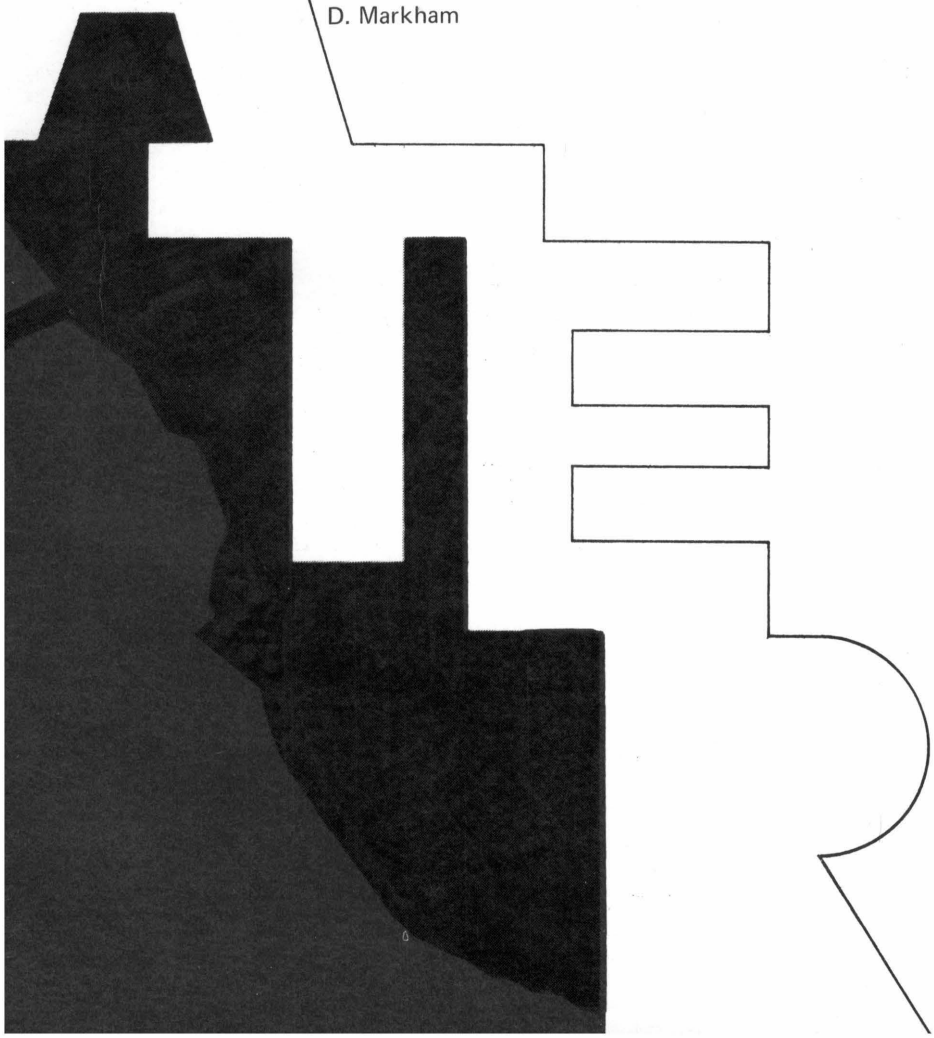

Bulletin 93
April 1976

Penetration and Mixing of Heated Discharges into Waterways

J. A. Schetz
C. H. Lewis
B. L. Sill
J. C. Chien
D. Markham

Aerospace and Ocean Engineering Department
Virginia Polytechnic Institute and State University

The work upon which this report is based was supported by funds provided by the United States Department of the Interior Office of Water Resources Research, as authorized by the Water Resources Resarch Act of 1964 (P.L. 88-379)

OWRT Project B-041-VA
and
OWRT Project B-054-VA
VPI-VWRRC-BULL 93

A publication of
Virginia Water Resources Research Center
Virginia Polytechnic Institute and State University
Blacksburg, Virginia 24061

TABLE OF CONTENTS

(continued)

LIST OF FIGURES

(continued)

ABSTRACT

This report contains the results of a series of related studies of thermal discharges into waterways and the resulting mixing zones. The first investigation involved the physical situation of a single, isolated horizontal jet discharge below the surface of a deep, moving channel. The results of laboratory experiments, approximate analysis and direct numerical solutions are reported for this physical situation. The second investigation considered the configuration of a tangential jet discharge along one bank of a shallow, moving channel. As with the first configuration, results are reported for laboratory experiments, approximate analysis and numerical solutions. In addition, limited comparisons between the predictions of the approximate analysis and some field measurements are provided. The third and final investigation was a comparative study of the effects of using three more types of injector geometries for thermal discharges—a multi-port diffuser, a single jet on the surface that is discharging perpendicular to the main channel flow, and a single jet resting on the channel bottom and also discharging perpendicular to the main flow. For these geometries, comparative data are provided on recirculation zones, hot spots, and surface temperature distributions.

INTRODUCTION

The environmental problems created by thermal pollution are of increasing concern to government, industry, and the public. The rejection of heat in industrial processes, as required by thermodynamics, has reached truly astronomical proportions. By far, the largest fraction of this waste heat results from electric power generation, and most of the total is discharged into waterways. By 1980, the water usage in the USA will be 250 billion gallons per day.

The most common system for heat disposal is the "once-through" method where water is discharged back into a waterway at 10 to 25° F above the intake value. While other methods for cooling, such as wet or dry cooling towers, have been proposed and, indeed, are in use, the simple once-through water cooling system enjoys much greater application, since it is the cheapest to build and operate.

The material in this brief introduction generally will not come as a surprise to the engineer or physical scientist, except that he probably was not fully aware of the magnitudes of total energy rejection involved. The real problem is created by the extreme sensitivity of biological systems to what the engineer or physical scientist would consider very small temperature variations. One can clearly see then, that this is an example of an environmental problem where heat transfer effects are dominant.

An emerging awareness of these problems has prompted many legislative bodies to enact controls on the allowable characteristics of the "mixing zone" produced by heated water discharges. This has created a need for accurate predictive analyses that can be used both by regulatory agencies and the design engineer in order to insure compliance and/or prevent expensive and time-consuming redesign and modification.

This report describes the development of two approximate, integral analyses, two exact numerical solution procedures, and supporting laboratory experiments. The text is organized in four separate sections.

STUDIES OF A SINGLE, HORIZONTAL JET IN A DEEP CHANNEL

I. Experimental Studies

The experiments were conducted in our laboratory, using a specially constructed facility. This facility, the instrumentation, methods of observation, and the results are described in the succeeding sections. Complete details are available in Sill and Schetz [1973].

A. Flow Channel

Following our exploratory work reported in Campbell and Schetz [1972 and [1973], it was decided that a larger and more convenient flow channel was necessary in order to conduct experiments more representative of actual field situations. The facility that resulted from our design study is shown in Figure 1. The channel is 2.0 feet wide with a maximum allowable depth of 1.5 feet and a measuring section length of 12.0 feet. The working sections are made entirely of Plexiglas to reduce heat losses and to permit flow visualization. The bottom and one side of these sections are ruled in 1.0 inch by 1.0 inch squares.

The inlet end of the channel is fitted with a sloped-bottom settling chamber and a flow-straightening section made of soda straws and screens. The flow enters the settling chamber through a header to provide spanwise distribution. This system produced a very uniform entrance flow in the channel.

The downstream end of the test section is terminated by a special control valve constructed of two plates with evenly spaced 1.0 inch holes. The rear plate can be slid with respect to the forward plate to permit flow area variation from 0 to 30 percent of the channel area.

After leaving the control valve, the flow is discharged into a reservoir which is connected back to the feed pump by a 3.0 inch plastic pipe under the channel. With this system, flow velocities of 0.05 to 0.5 feet per second can be used conveniently.

B. Injection System

The water injectant is dyed with food coloring and heated in an insulated aluminum tank (2.5 gallons) by means of a 150-watt electric heater. This tank also serves as a reservoir. The fluid is driven from the tank through a rotameter, a needle valve for control, and into the flow channel by means of air pressure. The connections are $^3/_8$ inch plastic tubing. Small plenum chambers for the injection ports are formed by counterboring the outside walls of the test section, 2.5 inches by 0.5 inches deep, and fitting a cap with a 2.5 inches by 0.5 inch deep recess over the opening. The tests reported here were performed with a 0.36 inch diameter injection port located

FIGURE 1
Layout of Water Channel

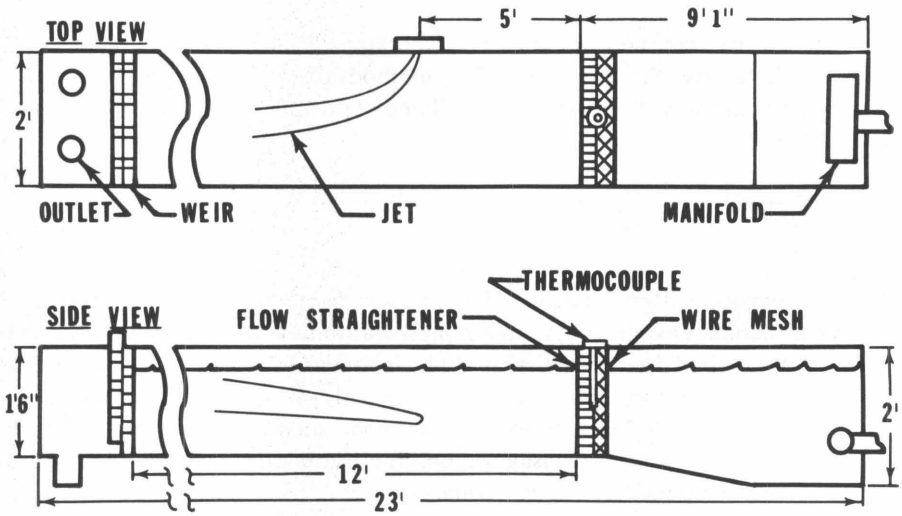

FIGURE 2
Short Duration Photo of Unheated Jet

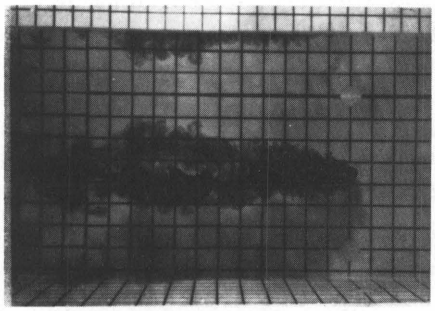

4.88 inches above the channel bottom and 5.0 feet downstream of the flow straightener. Injection is perpendicular to the main stream.

C. Instrumentation

The primary monitoring measurements necessary for these tests were the flow rates in the main channel and through the injection port, the temperature of the main stream, and the temperature difference between the main and injectant streams. The mass flow in the main channel was determined by an Annubar Flow Element located in the 3.0-inch intake line to the pump. The mass flow of the injectant was measured with a Fisher-Porter rotameter.

The temperature of the free stream and the injectant/free stream temperature difference were measured using Copper-Constantan thermocouples and an electronic ice-junction.

The photographs were taken with simultaneous exposures on two Graflex cameras using Polaroid type-51 film.

D. Results

A typical short duration ($^1/_{20}$ second) photograph is shown in Figure 2, where the turbulent structure and the characteristic vortex pair are clearly visible.

The primary test series of interest here was run with a $\Delta T = 80^\circ$ F and $V_j/V_\infty = 4.7$, 6.4 and 9.3. A "streak" photograph (4.0 seconds) as viewed from the side of the $V_j/V_\infty = 6.4$ case is shown as Figure 3. The vertical rise of the mixing zone due to buoyancy can be observed. The trajectories as determined from the center of the dye trace for the three cases are shown in Figure 4. The lines marked "Analysis" are the predictions of the approximate analysis to be described in the next section.

II. Approximate Analysis

The development of the approximate analysis has been presented in Campbell and Schetz [1972] and verified by comparison with experiment for cases with a two-dimensional (i.e. in-plane) trajectory in Campbell and Schetz [1973]. A summary presentation of the major features and approximations of the work will be given here. This will be followed by comparisons of predictions with the current three-dimensional trajectory experments.

The integral approach is used with a control volume formed by the total area of the mixing zone and a differential length along the trajectory. The origin of the cartesian (x,y,z) axis system is at the injection point, while the natural (s,n,t) axis system moves and rotates as it follows the path of the jet axis traced out by the jet velocity.

FIGURE 3
Streak Photo of Heated Jet
($\Delta T = 80^\circ$ F, $V_j/V_\infty = 6.4$)

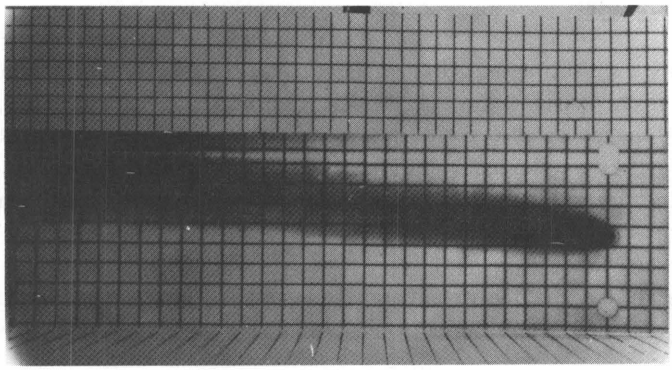

The equations expressing conservation of mass, momentum, and energy in the direction of the natural axes are applied to this control volume. The values of the dependent variables (velocity, density, and temperature) are taken as uniform over the cross-sectional area of the jet at any point along the trajectory.

For this system, conservation of mass may be written simply as a statement that the rate of change of mass in the control volume equals the entrainment of free stream fluid per unit length, into the mixing zone. We have used air jet experiments to develop an empirical relationship [Campbell and Schetz, 1972].

The general integral momentum equation is resolved into the "s," "n," and "t" directions to give three momentum equations. For the "n" and "t" directions, the shear and pressure forces are combined into a drag force which is calculated using a drag coefficient estimated from solid body data applied to this "equivalent solid body." Values of $C_{Dn} = 1.6$ and $C_{Dt} = 1.0$ were used which are consistent with the assumed 5:1 elliptical shape of the jet cross-section.

For the "s" momentum equation, it was necessary to model the shear and the pressure gradient along the jet trajectory. The details of the required assumptions are contained in Campbell and Schetz [1972].

Finally, the integral energy equation is used to predict the rate of temperature decay. The cooling of the jet is accomplished by a combination of the entrainment of cooler, free stream fluid and convection heat transfer around the "equivalent solid-body" of the jet. The latter is calculated by an empirical formula from Eckert and Drake

FIGURE 4

Centerline Trajectories for Experimental Cases

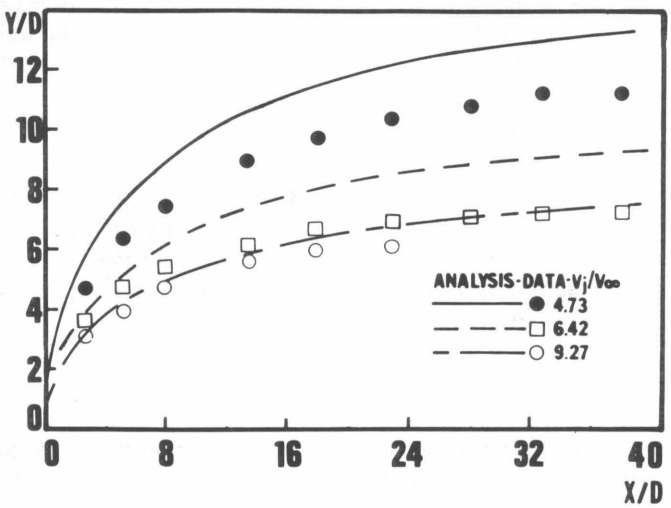

a. Projections on (X–Y) Plane

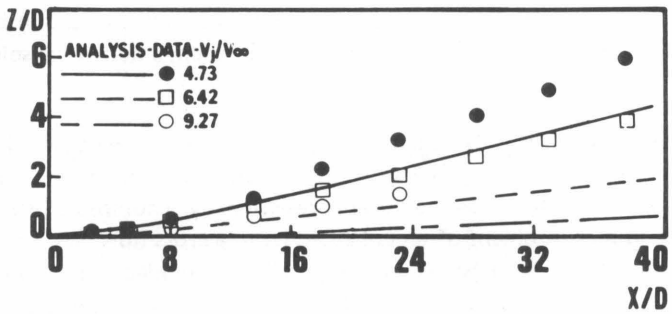

b. Projections on (X–Z) Plane

[1959]. The importance of both phenomena was shown in Campbell and Schetz [1973], along with a demonstration of the accuracy of the representation used.

The predictions of the analysis are compared with the data for the three experimental cases in Figure 4 in terms of the projections of the three-dimensional trajectories on the x-y and x-z planes. The cross-stream penetration is relatively well predicted for the highest and lowest velocity ratio cases. In general, the effects of buoyancy forces, as manifested by the curvature of the jet trajectory out of the injection (x-y) plane, are underestimated. The best results, overall, were obtained for the highest velocity ratio case. It is well to note at this point that there were no free constants in the analysis which were adjusted to match the data. Further detailed measurements in such three-dimensional trajectory cases will, however, permit the refinement of some assumptions, such as the assumed 5:1 shape of the jet cross-section, which might result in improved predictions.

III. Numerical Solution

At best, the integral approach used in the previous section is capable of predicting gross properties of the flow such as the trajectory and average values of the temperature along the trajectory. Detailed temperature and velocity patterns can be obtained only with a differential formulation. Considering the three-dimensional nature of the problem, and the fact that the direction of the most rapid rate of change varies in different regions of the flow, it is clear that a representation based upon the Navier-Stokes equations is required. Obviously then, a numerical solution must be utilized.

Within a general numerical treatment, a steady solution can be obtained by either a steady formulation or by considering the asymptotic result of an unsteady formulation. An attempt at the latter has been presented by Thompson [1971] for the related, but simpler, problem of an unheated jet in a cross-flow. We have adopted a steady formulation of the basic equations and have extended the general numerical procedure developed by Goseman, Spalding, et al. for two-dimensional cases to the present three-dimensional flow. Also, Spalding worked with a stream function vorticity formulation, while we have used velocity vorticity. Complete details of the development are contained in Chien and Schetz [1973] and Chien [1973].

A. Differential Equations

For a channel flow problem, the appearance of several boundary walls makes the determination of the pressure distribution very difficult. In this case, the pressure distribution is known only at an upstream station and at the free surface. For the rest of the flow field, it can be obtained only through the solution of the differential equations. Therefore, it is convenient to remove the pressure term from the governing equations, and this can be done with the introduction of vorticity by taking the curl operation on the momentum equation.

Ω_x –vorticity equation:

$$\frac{\partial^2}{\partial x^2}(\nu\Omega_x) + \frac{\partial^2}{\partial y^2}(\nu\Omega_x) + \frac{\partial^2}{\partial z^2}(\nu\Omega_x) - \left(u\frac{\partial\Omega x}{\partial x} + v\frac{\partial\Omega x}{\partial y} + w\frac{\partial\Omega x}{\partial z}\right)$$

$$= \frac{1}{\rho}\left(\frac{\partial F_z}{\partial y} - \frac{\partial F_y}{\partial z}\right) + \left\{-\Omega_x\frac{\partial u}{\partial x} + \frac{\partial w}{\partial x}\frac{\partial u}{\partial y} - \frac{\partial v}{\partial x}\frac{\partial u}{\partial z}\right\} + \frac{\partial}{\partial x}\left(\nabla\cdot[\nu\vec{\Omega}]\right) \quad [1]$$

Ω_y –vorticity equation:

$$\frac{\partial^2}{\partial x^2}(\nu\Omega_y) + \frac{\partial^2}{\partial y^2}(\nu\Omega_y) + \frac{\partial^2}{\partial z^2}(\nu\Omega_y) - \left(u\frac{\partial\Omega y}{\partial x} + v\frac{\partial\Omega y}{\partial y} + w\frac{\partial\Omega y}{\partial z}\right)$$

$$= \frac{1}{\rho}\left(\frac{\partial F_x}{\partial z} - \frac{\partial F_z}{\partial x}\right) + \left\{-\Omega_x\frac{\partial v}{\partial y} + \frac{\partial v}{\partial z}\frac{\partial u}{\partial y} - \frac{\partial v}{\partial x}\frac{\partial w}{\partial y}\right\} + \frac{\partial}{\partial y}\left(\nabla\cdot[\nu\vec{\Omega}]\right) \quad [2]$$

Ω_z –vorticity equation:

$$\frac{\partial^2}{\partial x^2}(\nu\Omega_z) + \frac{\partial^2}{\partial y^2}(\nu\Omega_z) + \frac{\partial^2}{\partial z^2}(\nu\Omega_z) - \left(u\frac{\partial\Omega z}{\partial x} + v\frac{\partial\Omega z}{\partial y} + w\frac{\partial\Omega z}{\partial z}\right)$$

$$= \frac{1}{\rho}\left(\frac{\partial F_y}{\partial x} - \frac{\partial F_x}{\partial y}\right) + \left\{-\Omega_z\frac{\partial w}{\partial z} + \frac{\partial w}{\partial x}\frac{\partial v}{\partial z} - \frac{\partial w}{\partial y}\frac{\partial u}{\partial z}\right\} + \frac{\partial}{\partial z}\left(\nabla\cdot[\nu\vec{\Omega}]\right) \quad [3]$$

With the introduction of the vorticity, a set of equations for v, u, and w can be derived from the original continuity equation. The three derived equations are then used to replace the original role of the continuity equation.

By taking partial derivatives of the continuity equation, and rearranging, we get:

$$\frac{\partial^2 u}{\partial x^2} + \frac{\partial^2 u}{\partial y^2} + \frac{\partial^2 u}{\partial z^2} = \frac{\partial\Omega_y}{\partial z} - \frac{\partial\Omega_z}{\partial y} \quad [4]$$

$$\frac{\partial^2 v}{\partial x^2} + \frac{\partial^2 v}{\partial y^2} + \frac{\partial^2 v}{\partial z^2} = \frac{\partial\Omega_z}{\partial x} - \frac{\partial\Omega_x}{\partial z} \quad [5]$$

$$\frac{\partial^2 w}{\partial x^2} + \frac{\partial^2 w}{\partial y^2} + \frac{\partial^2 w}{\partial z^2} = \frac{\partial\Omega_x}{\partial y} - \frac{\partial\Omega_y}{\partial x} \quad [6]$$

Equations [1] –[6] constitute a new set of governing equations without the appearance of the pressure term.

We have used the Energy equation in the form:

$$u\frac{\partial T}{\partial x} + v\frac{\partial T}{\partial y} + w\frac{\partial T}{\partial z} = \frac{1}{\rho C_p}\left(\frac{\partial}{\partial x}\left(K\frac{\partial T}{\partial x}\right) + \frac{\partial}{\partial y}\left(K\frac{\partial T}{\partial y}\right) + \frac{\partial}{\partial z}\left(K\frac{\partial T}{\partial z}\right)\right) \quad [7]$$

where the assumption of negligible viscous dissipation and pressure work has been used.

With the vorticity formulation, the specification of boundary conditions is not trivial. The reader is referred to Chien and Schetz [1973] for the necessary details. The downstream boundary condition was taken as a "parallel flow."

B. Numerical Solution Procedure

The differential equations were put in finite difference form by integration over an elementary control volume. Various means of approximating the resulting integrals to produce different finite difference forms were investigated, in detail, for convection terms, source terms, and diffusion terms. The final formulation selected is essentially equivalent to "upwind differencing."

The system of algebraic equations that results from the finite differencing operations is complex and very large for the problem of interest here. In this situation, an iterative method is mandatory, and we have selected point over-relaxation.

C. Additional Assumptions

Since the jet is turbulent in most cases, a simple turbulent eddy viscosity model has been employed. Although one of the more sophisticated approaches (e.g. Launder and Spalding [1972] or Harlow [1973]) could be incorporated, it was felt at this state of development of the procedure, that the proposed model was adequate to describe the primary features of the flow. Further, little of the detailed turbulent data needed for the more complicated approaches is available for this problem.

The Prandtl eddy viscosity model for axi-symmetric jets,

$$\epsilon = 0.0256\,(V - V_\infty)\,b_{1/2}\ ,$$

was adopted as

$$\epsilon = 0.0256\,\frac{d_j}{2}\,(V_j - V_\infty)\ .$$

The rational for this assumption is given in detail in Chien and Schetz [1973]. The turbulent Prandtl Number was taken as 0.8.

A simplified free surface was also introduced in the formulation. It was assumed to be a flat plane which allowed velocity slip.

FIGURE 5

Temperature Profiles from Numerical Solution

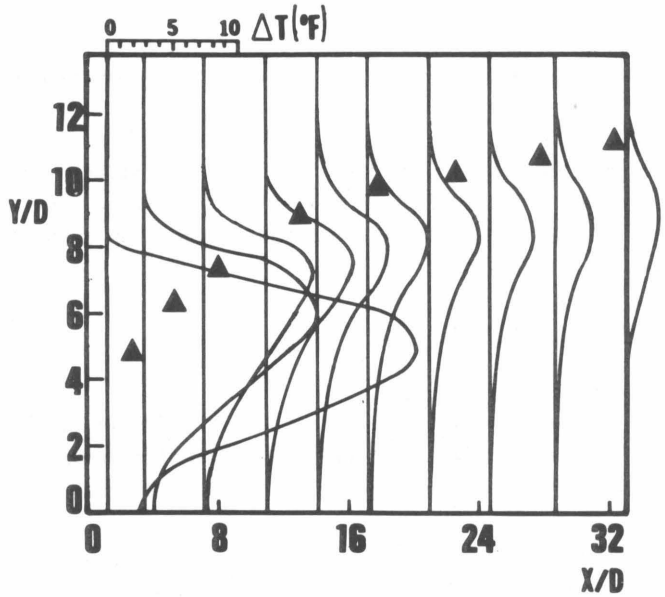

a. Projections on (X–Y) Plane

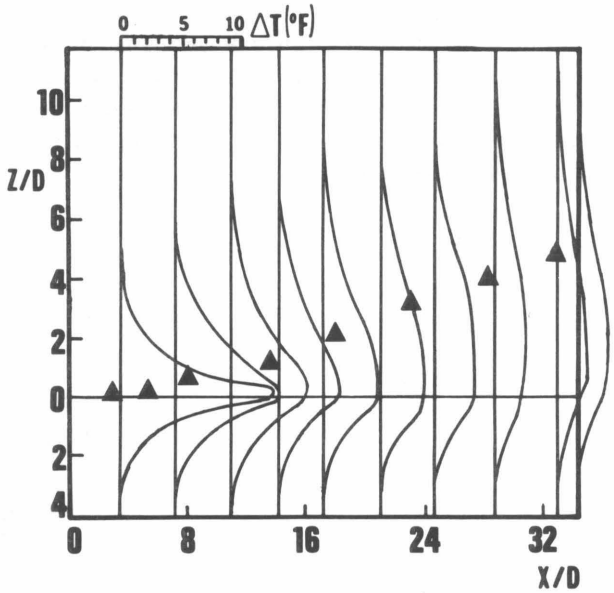

b. Projections on (X–Z) Plane

Finally, the classical Boussinesq approximation was used to model the buoyancy force due to the temperature variation in the flow field.

D. Test Case

In order to verify the accuracy of the numerical procedure developed here for problems of the type under study, a comparison was made between the predictions of our procedure and the experimental data of Goldstein and Kreid [1967] for the laminar flow in the entrance region of a square channel. Excellent results in terms of the centerline velocity variation and velocity profiles across the channel in the developing region were obtained. Detailed comparisons are given in Chien and Schetz [1973].

E. Comparison with Experiment

Calculations were run for the experimental case with $V_j / V_\infty = 9.3$, and the results are presented in terms of temperature profiles in Figures 5a and 5b. Also shown for comparison are the appropriate projections of the center of the dye traces as observed from experiment.

The shape of the profiles is revealing in that they display the effects of the non-uniform cooling of the jet due to "sheltering" in various regions of the flow. This is particularly pronounced in the x-y plane projection.

While the comparison of the center of a dye trace and temperature profiles is not direct, some assessment of the accuracy of the predictions can be made on this basis. From this comparison, it appears that the numerical solution underestimates slightly the penetration of the jet both across the stream and towards the surface. Further development of the simple turbulence model employed can be expected to improve the predictions of the details of the flow.

STUDIES OF A TANGENTIAL JET INTO A SHALLOW CHANNEL

I. Experimental Studies

A. Flow Channel

The same basic channel that was described in the previous Experimental Studies section was used here also. In this case, the injector, placed on one sidewall of the channel, had a $^{7}/_{8}$ inch opening extending from the bottom to within $^{1}/_{8}$ of the surface, and out from the wall 0.22 inches, so that the initial channel-to-jet width ratio was approximately 100:1.

B. Instrumentation

Flow visualization techniques were employed to provide direction for the detailed temperature and velocity measurements. Photographs for these tests were obtained with two Graflex 4 inch by 5 inch cameras mounted in tandem a distance of four feet above the channel. This provided a field of view which included the entire channel width and a streamwise distance of six feet, or three channel widths. Various dye techniques were used, and these will be described as the results are presented in succeeding sections.

Detailed jet temperature measurements were made with a specially constructed thermocouple rake consisting of six equally spaced, vertically aligned, sheathed thermocouples ($^{1}/_{16}$ OD) which covered the entire free stream depth. A conical hot film probe (Thermosystems Model 1050) was used in conjunction with a temperature-velocity switching circuit to obtain velocity values in the highly non-isothermal buoyant injection runs. In the following sections, data for unheated injection will be presented prior to that for heated jets, allowing the two complicating factors of boundedness and buoyancy to be examined in turn.

C. Results

The horizontal spread of both unheated and heated jets was obtained photographically by injecting water dyed with food coloring. Time exposures (6 seconds) were used to smooth the outer jet boundary and facilitate spread measurements. A maximum of five and minimum of two photos were taken at each set of conditions, and no two runs were made consecutively at the same conditions. Using this procedure, maximum spread deviation was never greater than 10 percent of the mean.

The most dominant feature evident in the photographs of unheated jets was the large-scale eddies which caused most of the jet growth. Although these eddies were large, it was obvious from visual observations and from some of the photographs, that the near wall had a definite damping effect on them. The outer edge of the jet had an irregular sawtooth appearance, but the inner portion near the wall gave no

FIGURE 6

Flow Visualization with Dyed Injection,
U_1 = 3.0 inches per second and U_1/U_2 = 7.0

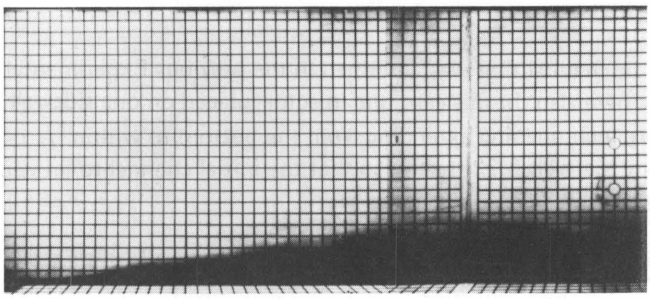

a. $\Delta T = 0^\circ$ F

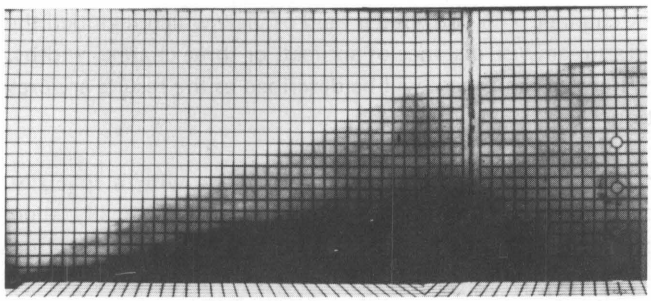

b. $\Delta T = 15^\circ$ F

FIGURE 7

Spread Measurements for Unheated Jets,
U_1 = 3.0 inches per second

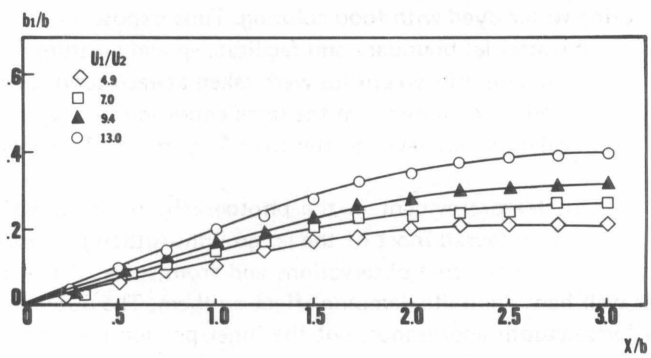

indication of turbulent "puffs" or eddies. Even though these eddies were damped, their size was of the same order as the jet width, thus verifying an assumption of classical mixing length approaches to jet flow problems. Figure 6 gives a typical time exposure of $\Delta T = 0$ injection, and Figure 7 presents jet spread normalized by the channel width b, for the unheated cases studied with $U_1 = 3$ inches per second. Similar data of other values of the free stream velocity are given in Sill and Schetz [1973]. Clearly evident is an increase in spread resulting from a decrease in free stream velocity.

Results for the heated jet were treated in essentially the same manner as for the unheated ones, although there was one basic difference. When the jet is buoyant, the bottom rises and the lateral jet spread is enhanced. Since the jet and free stream densities are different, the hydrostatic pressure forces are not balanced, with the result that the bottom will be forced upward and the outer vertical side inward at the bottom. After a small increment of time, the jet cross-section will appear rectangular with a triangular outer lip. When viewed from above, the jet at intermediate stations has a dark core and a greyish lip which gradually merge, as evidenced by the uniform dye intensity at downstream locations. For cases where this effect was pronounced (Figure 6b) data from the photographs were reduced to show the spread of both the core and lip.

Close examination of the turbulent structure of the jet showed that the density currents tended to suppress the turbulent eddies which were so obvious for unheated injection, and the jet-free stream interface was noticeably smoother than before. The eddies were no longer random but in more or less parallel rows and elongated in a downstream direction oblique to the near wall.

Jet spread reduced from the photographs for several cases is shown in Figure 8. As would be expected, an increase in U_2 or decrease in ΔT tends to decrease the spread. The two lines for $T = 30^\circ$ F, $U_1/U_2 = 4.9$ result from the core and lip (discussed above) and the backwards pointing line for $\Delta T = 30^\circ$ F, $U_1/U_2 = 13.0$ is due to a recirculation region in the free stream which will be discussed later.

The most direct effect of buoyancy is to enhance the jet spread. Spread at stations near the outfall, where the jet momentum is still large, is little affected by temperature increases, whereas it is changed markedly at stations further downstream where buoyancy is of primary importance.

The most startling effect observed, is the presence of a "dark zone" far downstream under certain heated injection conditions. This is an easily seen and reproduced, consistently-sized phenomenon, as shown in Figure 9. From the study of these photographs, it is evident that the zone consists of dyed jet fluid which extends to a greater depth than other portions of the surrounding jet.

FIGURE 8

Measured Spread of Heated Jets
with U_1 = 3.0 inches per second

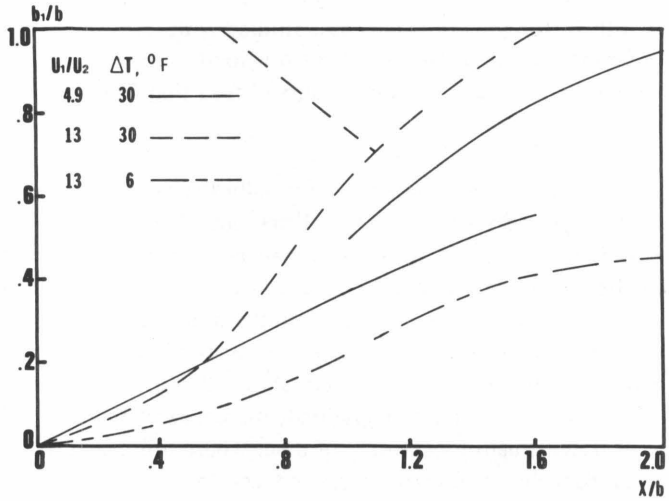

FIGURE 9

Flow Visualization with Dyed Injection,
U_1 = 3.0 inches per second, U_1/U_2 = 13.0, and $\Delta T = 30^\circ$ F

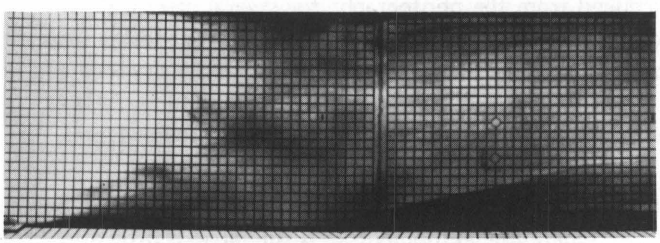

FIGURE 10
Visualization of the Flowfield,
U_1 = 3.0 inches per second, U_1/U_2 = 13.0, and $\Delta T = 0^\circ$ F

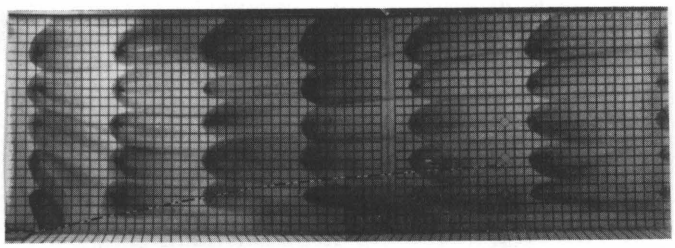

The free stream was laminar for all situations examined in the study, allowing the flow patterns to be studied by simple flow visualization methods. Since buoyant jets rise from the bottom and extend across the surface, it is desirable to use a method which gives flow direction on or near the channel bottom. With this in mind, dye tablets about ½ inch in diameter were placed on the bottom at regular intervals, thus providing a sensitive indication of free stream flow direction. For this portion of the study, neither the jet nor free stream was colored, thus allowing clear visualization of the flow patterns in the free stream in situations where the jet formed a layer across the surface. A thin line is placed on the photograph along the jet outline as determined from previous dyed injections. As before, the jet issues from the lower left corner in these photographs.

Figure 10 is typical of the flow field for $\Delta T = 0^\circ$ F injection. The most outstanding feature is angularity in the free stream flow caused by the jet entrainment as evidenced by the first spanwise row of dye tablets. Fluid closest to the jet is diverted most with the effect decreasing across the channel. Further downstream and near the far wall, the flow is angled slightly away from the jet, while nearer the jet, the flow is still deflected inward but not as steeply as in the first row of tablets.

Similar tests were also conducted using a heated injectant, and Figure 11 shows injection at the same velocities as Figure 10 but with $\Delta T = 30^\circ$ F. The first spanwise row of markers still evidences a strong entrainment, but now the entire flow is disturbed. At the far wall there is a recirculation bubble surrounded by the concentric streamlines, while at the near wall in the right side of the picture, dye from the wafers is drawn toward the wall and somewhat upstream. The free stream fluid is drawn toward the near wall as a result of jet entrainment. Then, in passing downstream of the recirculation bubble, the effective channel width increases, exposing the fluid to the same adverse pressure gradient found in diverging channels. It is well known that flow separation can occur as a result of such an effect, and this is precisely what happens to form the dark zone. On this basis, we would expect the

FIGURE 11

Visualization of the Flowfield,

U_1 =3.0 inches per second, U_1 / U_2 = 13.0, and ΔT = 30° F

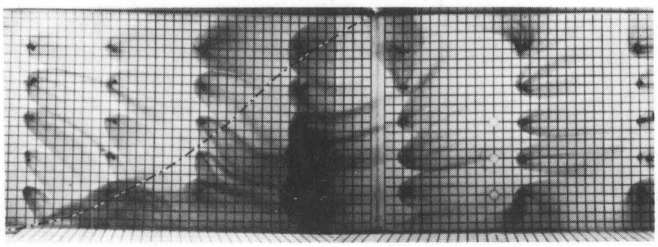

FIGURE 12

Isotherms in Channel Cross-section for

U_1 = 3.0 inches per second, U_1 / U_2 = 9.4, and ΔT = 15.0° F

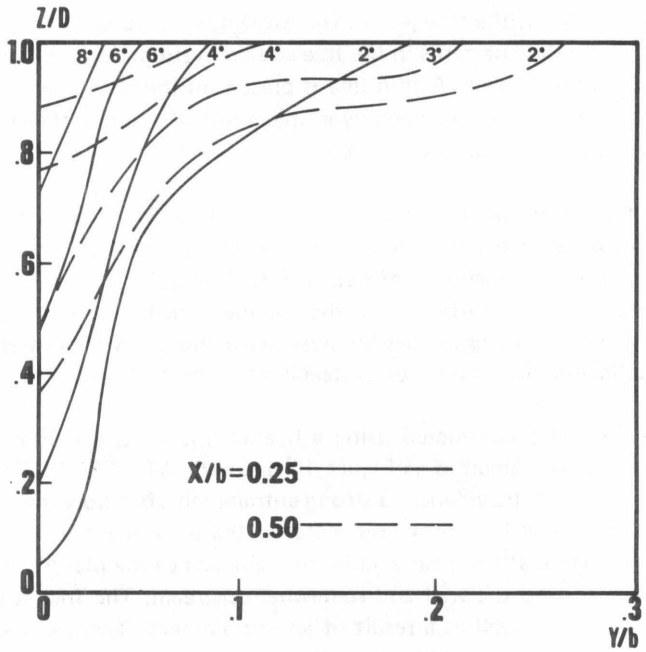

FIGURE 13
Surface Temperature Distributions,
$U_1/U_2 = 13.0, \Delta T = 30^\circ$ F

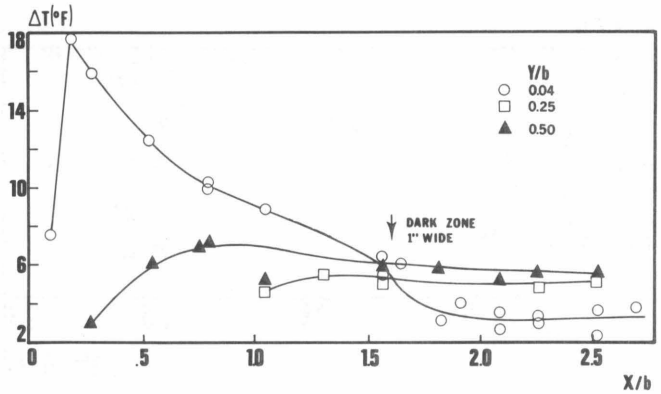

zone to have a low (or reversed) velocity which would promote mixing to a greater depth and cause the dark appearance as seen in Figure 9.

It is useful to examine temperature distributions for several jet cross-sections for comparison with conclusions drawn from the photographic study. The isotherms shown in Figure 12 reveal that the general jet shapes agree well with those reduced from the photographic survey and bear out the previous discussion of the core and lip.

To obtain some insight into the processes which occur in the "dark zone" encountered in the photographs, it is instructive to follow the downstream development of vertical temperature profiles as the zone is entered. For the case in Figure 11, the dark zone is three to four inches wide, so profiles were examined at a fixed spanwise coordinate of y = 1 inch. Before reaching the dark region, the two deepest thermocouples read $\Delta T = 0^\circ$ F, but after entering this zone, their readings increased to nearly 3° F. Obviously the flow field is such that some jet fluid is transported into the lower portions of the channel and this fluid carries with it both thermal energy and coloration.

Since the amount of energy in the jet is limited, any mixing of the jet with cooler fluid from below should result in a decrease in temperature of the warmer portions near the surface. This particular phenomenon is seen vividly by studying the streamwise decay of surface temperature (Figure 13). While the temperatures outside the dark zone decay gradually, a sharp drop is detected at y = 1 inch for the x station at which the zone width has grown to one inch.

FIGURE 14

Vertical Velocity Profiles,

U_1 = 3.0 inches per second, U_1 / U_2 = 13.0, and ΔT = 30° F

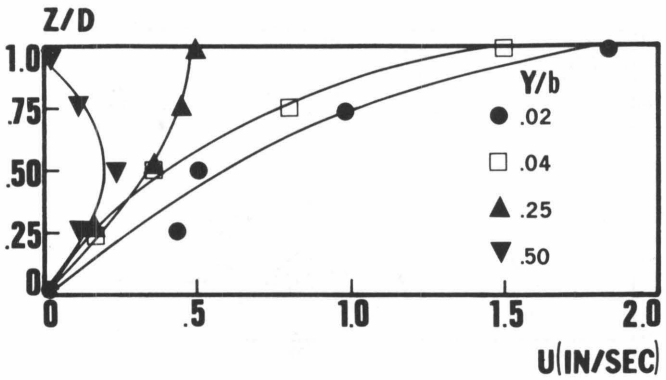

a. X/b = .25, b_1 / b = .125

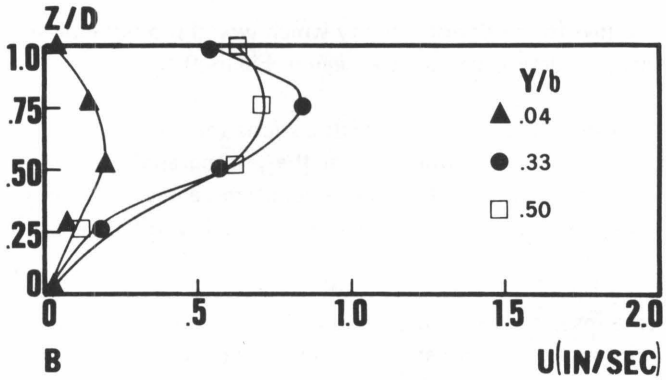

b. X/b = 2.17, b_1 / b = 1.0

FIGURE 15

Spanwise Velocity Profiles,

U_1 = 3.0 inches per second, U_1/U_2 = 13.0, and $\Delta T = 0^\circ$ F

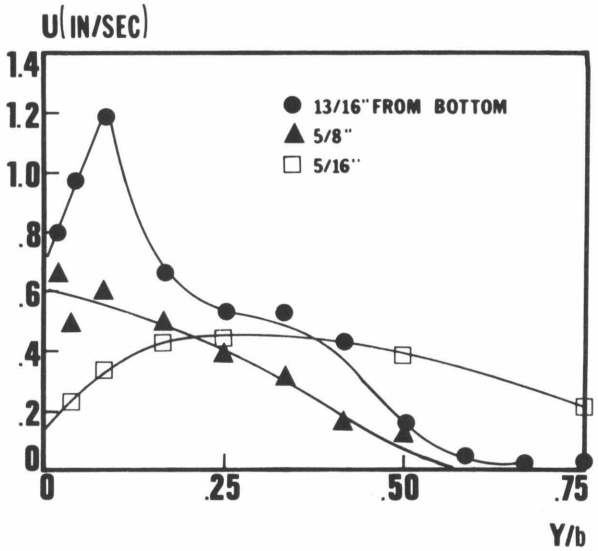

a.X/b = 0.50

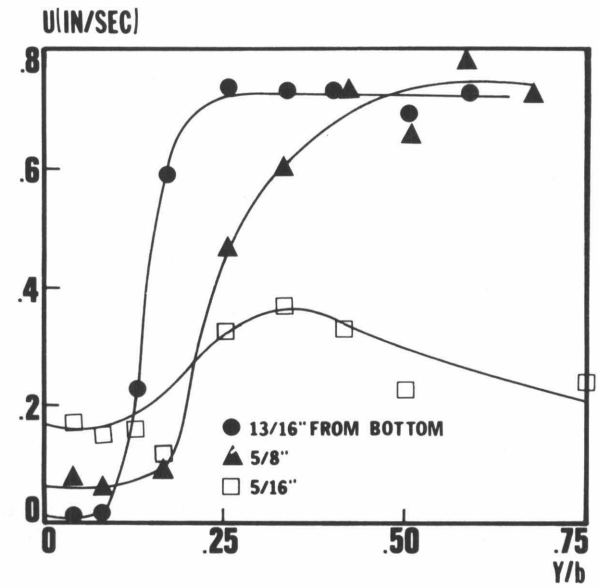

b. X/b = 2.17

As expected, the velocity profiles for $\Delta T = 0$ injection were primarily two dimensional. Horizontal profiles were Gaussian in shape (in accord with free jet results) and the decay of maximum velocity obeyed the inverse square root law predicted by classical free jet analyses. In summary, unheated injection produced no surprising results as regards the velocity distributions in the system.

Velocity results for heated injection will be presented for the case in Figures 9 and 11 which contain both a recirculation bubble and a separation region (dark zone). Figure 14a presents vertical profiles at the streamwise station where the jet is four inches wide. For the innermost y stations the velocity increases almost linearly. Moving out into the free stream, the surface velocities gradually decrease until at 12 inches the velocity has dropped essentially to zero. This is a direct consequence of the recirculation bubble seen in Figure 11.

The second set of profiles (Figure 14 b) were taken at $x = 52$ inches, which is well downstream of the start of the dark zone. At this station, the jet extended almost completely across the channel, and the separation region was about four inches wide. The very low velocities near the wall occur at the spanwise location where the maximum jet velocities were found upstream. Comparison of Figures 14a and 14b for $y = 1$ inch show a radical drop in velocity and change in the vertical profile from a to b. It is also obvious that the greatest change occurs in the upper half of the total depth. If the jet flow has actually separated from the near wall, the maximum channel velocity will be displaced outward. The two remaining curves in Figure 14b show a high velocity portion in the upper half of the fluid where the jet is located. It is thus apparent that the jet has simply been pushed away from the wall in this region.

Spanwise velocity profiles vary radically from the Gaussian shapes obtained for unheated injection. Figure 15 presents these curves at three depths for a streamwise position of 12 inches from the injector. Due to buoyancy effects, the maximum velocity occurs near the surface with a fairly rapid decrease both horizontally and vertically. Further out in the free stream the velocities near the surface are retarded much more than those slightly deeper, which is the same effect shown in Figure 14a, indicating that the recirculation region which is generated by the jet is strongest near the surface.

Moving downstream to 52 inches from the injector, the velocities vary markedly and the dark zone is very pronounced (Figure 15b). Near the wall, the velocities are very small with a large gradient occurring at the edge of the separation region. As evidenced by the vertical profiles, the gradients are largest near the surface and smaller in the interior of the fluid. In the dark zone the velocities are largest near the bottom, whereas outside this zone just the opposite is true. Also it is interesting to note that the spanwise velocity variation is quite small outside the separation region.

II. Approximate Analysis

A. Model Development

The simplified analysis developed here allows prediction of the gross physical and dynamic parameters of a rectangular, buoyant, surface jet discharged into a co-flowing, bounded mainstream. Since the minute details of this complex flow situation are not well known and the overall effects are important from a regulatory standpoint, an integral or control volume approach is useful. The control volumes are chosen such that the bounding walls are assumed vertical and parallel, and the free surface is of uniform depth across the entire channel. The jet is initially discharged at, and along, the near shore with the assumption that it retains a rectangular cross-section with varying width-to-height ratio and size as it proceeds downstream. A detailed description of the assumptions and manipulations required can be found in Sill and Schetz [1973]. Mass conservation may now be written as:

$$\frac{d}{dx}\left[\int_{S_1}\int \rho_1 u_1 \, dS\right] = e_1 \qquad [1]$$

for the jet, and

$$\frac{d}{dx}\left[\int_{S_2}\int \rho_2 u_2 \, dS\right] = e_2 \qquad [2]$$

for the main stream.

Momentum conservation may be written as

$$\frac{d}{dx}\left[\int_{S_1}\int \rho_1 u_1^2 \, dS\right] = e_1 u_2 + I_1 \qquad [3]$$

and

$$\frac{d}{dx}\left[\int_{S_2}\int \rho_2 u_2^2 \, dS\right] = e_2 u_2 + I_2 \qquad [4]$$

for the jet and main stream respectively, where

$$I_1 = \left[\int_{S_1}\int F_s \, dS + \int_{V_1}\iint F_b \, dV\right]$$

$$= -\rho_1 g b_1 D_1 \frac{dD_1}{dx} + \tfrac{1}{2} C_f \rho_{eq} u_{eq}^2 \left(\frac{\dot{m}_1}{\dot{m}\bar{u}_1} - \bar{u}_1^2 \bar{\rho}_1 \frac{A_{1w}}{A_w}\right)(b + 2D) \qquad [5]$$

and

$$I_2 = -\rho_2 g(Db_2 + b_1 D_2)\frac{dD}{dx}$$

$$+ \tfrac{1}{2}C_f \rho_{eq} u_{eq}^2 \left(\frac{\dot{m}_2}{\dot{m}u_2} - |\bar{u}_2|(\bar{u}_2)\bar{\rho}_2 \frac{A_{2w}}{A_w}\right)(b + 2D) \qquad [6]$$

where the "bar" denotes nondimensionalization with respect to the equilibrium values ρ_{eq} or u_{eq} as appropriate.

In a similar manner, the energy equation becomes

$$\frac{d}{dx}\left[\int_{S_1}\int \rho_1 C_V T_1 u_1 \, dS\right] = e_1 C_V T_2 + \int_{A_1}\int (Q_i/\Delta x)\, dA \qquad [7]$$

for the jet, and

$$\frac{d}{dx}\left[\int_{S_2}\int \rho_2 C_V T_2 u_2 \, dS\right] = e_2 C_V T_2 + \int_{A_2}\int (Q_i/\Delta x)\, dA \qquad [8]$$

for the main stream, with

$$Q_1 = h(b_1 \Delta x)(T_a - T_1) \qquad [9a]$$

and

$$Q_2 = h(b_2 \Delta x)(T_a - T_2] \qquad [9b]$$

A careful enumeration of the equations and unknowns reveal that seven additional relations are needed for closure. Two are immediately obvious from geometric considerations, or

$$b_1 + b_2 = b \qquad [10]$$

and

$$D_1 + D_2 = D \qquad [11]$$

and two more from the equation of state

$$\frac{\partial \rho_1}{\partial T_1} + C_T = 0 \qquad [12]$$

and

$$\frac{\partial \rho_2}{\partial T_w} + C_T = 0 \qquad [13]$$

in which C_T, the coefficient of thermal expansion, was assumed constant, providing a locally, linear temperature-density relationship. Global continuity is expressed as

$$e_1 + e_2 = 0 \qquad [14]$$

The remaining two equations are obtained by modeling the change in jet depth and width in terms of other unknowns. Assuming the effects of mixing, friction, and buoyancy induced density currents are independent, and the growth models are obtained as the sum of the above contributions [Sill and Schetz, 1973a] . Thus we find

$$\frac{db_1}{dx} = \frac{b_2}{b}\left(1 - \tfrac{1}{2}\frac{b_1}{b}\right)\left[C_j \frac{(u_1 - u_2)}{|u_1| + |u_2|} + \frac{b_1}{D_1}\frac{C_b}{F_r} - \frac{b_1}{2}\frac{G_1}{\dot{m}_1 \bar{u}_1}\right] \qquad [15]$$

and

$$\frac{dD_1}{dx} = \frac{D_2}{D}\left(1 - \tfrac{1}{2}\frac{D_1}{D}\right)\left[C_j \frac{(u_1 - u_2)}{|u_1| + |u_2|} + C_j C_b \frac{b_2}{b}\left(1 - \tfrac{1}{2}\frac{b_1}{b}\right)\frac{b_1}{D_1 Fr} - \frac{D_1}{2}\frac{G_1}{\dot{m}_1 \bar{u}_1}\right] - \frac{b_2}{b}\left(1 - \tfrac{1}{2}\frac{b_1}{b}\right)\frac{C_b}{F_r} \qquad [16]$$

where

$$G_1 = \tfrac{1}{2} C_f \rho_{eq} u_{eq}\left[\frac{m_1}{\dot{m}\bar{u}_1} - u_1^2 \rho_1 \frac{A_{1w}}{A_w}\right] A_w \qquad [16a]$$

and where the depth expression contains a cross product term resulting from turbulent mixing caused by the density currents. The value of $C_j = 0.22$ [Abramovich 1962] is well established in the literature from free turbulent jet analyses; thus it remains to evaluate C_b, the only new constant introduced in the present analysis. In these expressions, the Froude number is:

$$Fr = \frac{u_2}{\sqrt{\frac{\Delta\rho}{\rho} g D_1}} \qquad [17]$$

It now remains to determine C_b in such a way that direct curve fitting is eliminated. If $\bar{u}_1 = \bar{u}_2$, the equations are greatly simplified, and may be readily integrated for average values of jet depth, D_1, to obtain

$$C_b = \frac{Fr_o \sqrt{D_1 / D_{1o}}}{(x/D_{1o})} \ln\left[\left(\frac{b_1}{b_{1o}}\right)\left(\frac{b_{2o}}{b_2}\right)^3 \left(\frac{1 - \tfrac{1}{2}(b_1/b)}{1 - \tfrac{1}{2}(b_{1o}/b)}\right)\right] \qquad [18]$$

Now, using this expression in conjunction with experimental measurements of b_1 and D_1 as a function of x, it is a straightforward process to plot C_b as a function of x with the result that C_b is asymptotic to 0.13, the value used throughout this study.

FIGURE 16

Effect of Temperature on Jet Spread for

U_1 = 3.0 inches per second

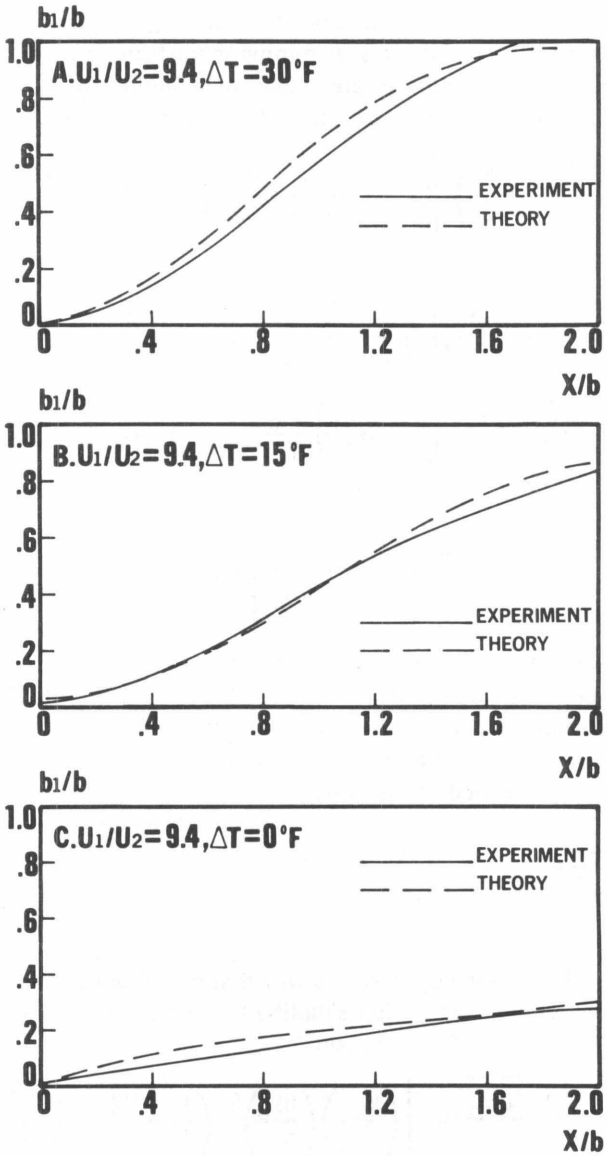

Velocity and temperature profiles must be specified before the actual solution can be obtained. This is an open choice and can be made as exact as knowledge of the flow allows. In the present case, there is little *a priori* information on which to base reasonable profiles, so reliance upon the insensitivity of integral methods to profile choices allowed use of simple, top-hat or slug velocity and temperature profiles.

B. Comparison with Laboratory Experiment

Theoretical predictions of the effect of temperature on jet spread are shown in Figure 16 for a typical velocity ratio. The spread changes markedly with small temperature changes, and good agreement was obtained for all cases.

Comparisons of the predictions of this analysis with laboratory studies over a wide range of conditions have been very good [Sill and Schetz, 1973]. This included good predictions of the combinations of conditions that produce recirculation in the main stream.

C. Comparison with Field Data

Calculations have recently been run for comparison with field observations. A typical example of the results is shown in Figures 17a and 17b. The analytical results for surface isotherms shown in Figure 17a agree well with the data from aerial infrared photographs shown in Figure 17b. We take this as further, strong substantiation of the adequacy of the analysis.

III. Numerical Solution

The basic numerical approach described in the previous Numerical Solution section was applied to the shallow channel geometry of interest in this section.

A. Eddy-Viscosity Model

A two-dimensional kinematic eddy-viscosity model that was nonconstant in the horizontal plane (x,y) was developed and used. The specific form applied was:

$$\epsilon^+ = \frac{\epsilon}{\rho} = .0081\,\delta^2 \left(\left(\frac{\partial u}{\partial y} \right)^2 + \left(\frac{\partial v}{\partial x} \right)^2 \right)^{1/2} \gamma \qquad [19]$$

where γ is Klebanoff's intermittency factor and δ is the jet half-width. For the numerical calculations δ was obtained using a least squares fit. Further details are provided in Markham [1975].

FIGURE 17

Surface Isotherm Pattern for Dan River Steam Station

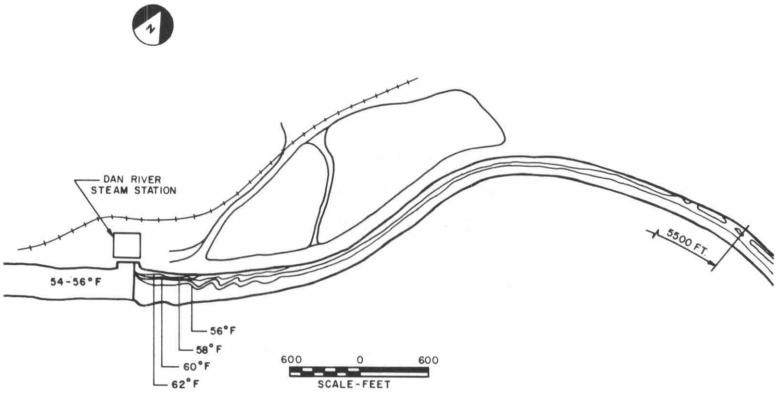

a. Measured by Aerial Infrared Photos

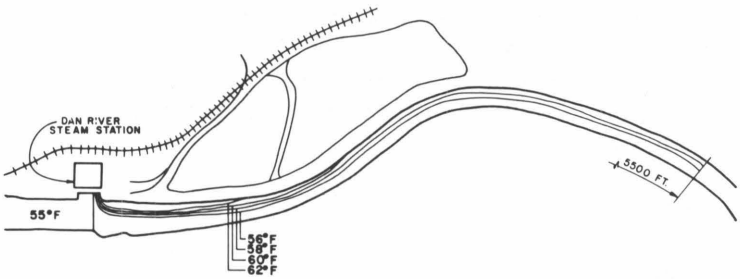

MAR. 13, 1973

PLANT INTAKE TEMP	- 55° F
PLANT DISCHARGE TEMP.	- 70° F
PLANT CONDENSER FLOW	- 434 CFS (UNITS 1-3, 2 PUMP OPERATION)
TOTAL RIVER FLOW	- 2818 CFS (MARCH 13, 1973 USGS)
PLANT LOAD	- 100% (290 MW)

b. Calculated

FIGURE 18
Spreading of an Unheated Jet

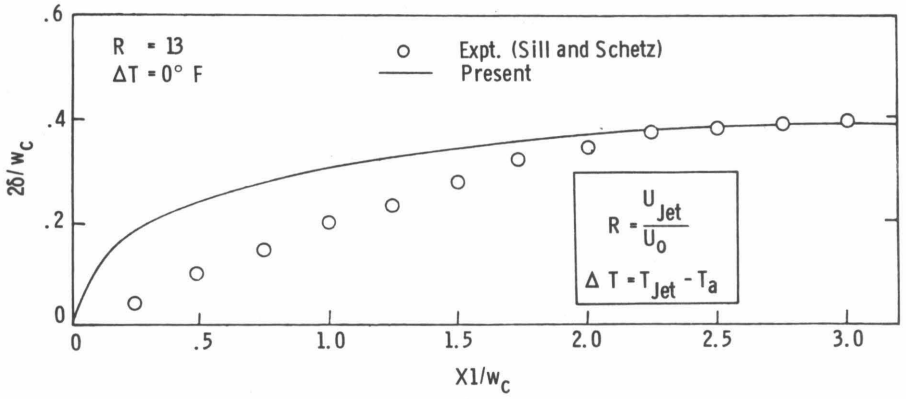

B. Energy Transport Model

Γ_e/ρ may be expressed as:

$$\frac{\Gamma_e}{\rho} = \frac{Pr_t + \epsilon^+ Pr}{Pr\ Pr_t} \qquad [20]$$

where Pr is the laminar Prandtl number and P_{rt} is the turbulent Prandtl number which is approximately 0.8 for liquids.

C. Turbulent, Unheated, Rectangular Jet into a Shallow Open Channel

The numerical model and program were tested further before the actual turbulent, heated jet case was run. This was done by running a turbulent, unheated jet case and comparing the results to those obtained experimentally and described in a previous section. The effect of the term, $\partial\nu_e/\partial_y \cdot \partial\Omega_y/\partial_z$, in the Ω_z-vorticity equation was also checked. The unheated case took approximately 120 iterations to converge (a good initial guess was used) at an average time of 1.3 minutes per iteration.

Briefly, the results were as follows. The term containing the eddy-viscosity gradient, $\partial\nu_e/\partial_y \cdot \partial\Omega_y/\partial_z$, noticeably increased the spread of the jet. Figure 18 compares the spread of the jet for the present result to the experimental result. The agreement is very good at distances greater than 2.1 channel widths downstream. At distances less than this, the present result increasingly overpredicts the jet spread as the jet entrance is approached. This overprediction was chiefly due to the modified jet velocity, which was used to restore information lost at the leading edge of the jet. This "overprediction" could be reduced by using a finer grid system in the jet system.

FIGURE 19
Spreading of a Heated Jet

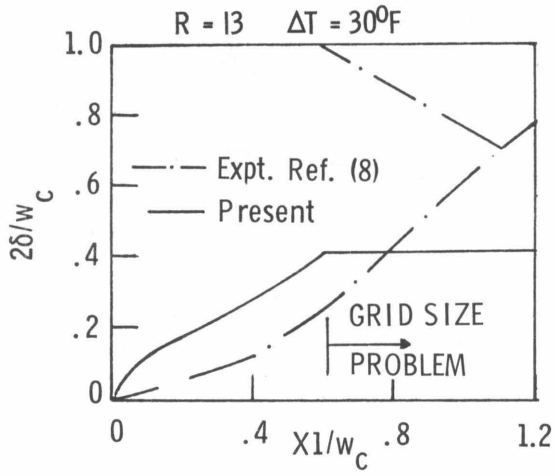

FIGURE 20
Velocity Vector Plot in the Cross Plane

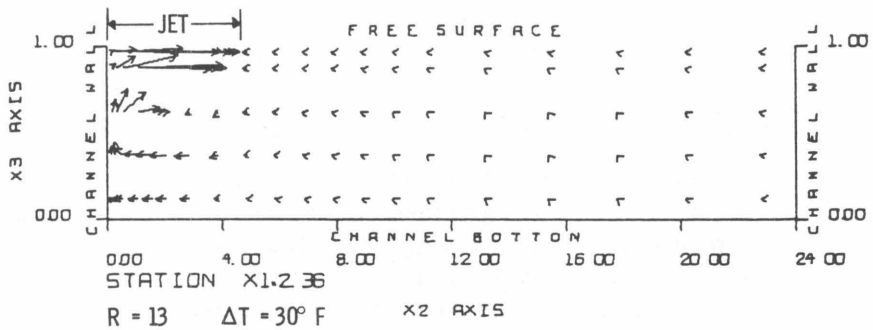

D. Turbulent, Heated, Rectangular Jet into a Shallow Open Channel

The input parameters for the case of the turbulent, three-dimensional, heated, rectangular jet were identical to those of the unheated case, with the exception of the jet temperature and its related parameters—namely, the coefficient of volumetric expansion, β, and the laminar Prandtl number, Pr.

The calculations for this case took approximately 1.6 minutes per iteration and were continued until the maximum relative changes of the free stream velocity (u) and temperature were respectively less than 0.1 and 0.005 percent between successive iterations. This took approximately 750 iterations, when a previous solution was used as the initial guess. The computation time for the heated case was greater than that of the unheated case due to the increased number of points in the vertical direction and the added complexity of the fluid flow due to the jet's buoyancy.

The grid system used for this case was nonuniform in all three directions; it consisted of 49 points downstream, 28 points across the channel, and 11 points from the bottom to the free surface.

In order to improve the stability of the numerical method, a laminar viscosity that was six times that of water at 68° F was used. To compensate for this increase, the properties of a 52.5 percent solution at 68° F of aqueous glycerol were used, since its laminar viscosity would not have a very large effect upon the overall comparisons with the experimental data, as the phenomena of interest were due mainly to the turbulence of the fluid.

Figure 19 compares the spread of the jet for the present result to the experimental results of the previous section. The agreement was reasonable up to 0.6 of a channel width downstream. At distances greater than this, the jet spread is grossly underpredicted by the present result. The reason for this large underprediction appeared to be due to the grid spacing in the vertical direction. The scale of the grid spacing appeared to be greater than that of the jet thickness at and near the free surface.

Although the jet spread was underpredicted in the downstream region for the present result, other flow field phenomena, such as the rise and spread of the jet or the free surface, and the entrainment of freestream fluid into the jet, are clearly observed in Figure 20. Figure 20 is a velocity vector plot in a cross-sectional plane of the channel two to six inches ($\approx$ 11 jet widths) downstream from the jet entrance.

Figure 21 is a plot of various isotherms (ΔT = constant) in the horizontal plane of the free surface. The isotherms with the highest values are restricted to a very small core of the jet. The boundary layer along the wall also showed up clearly in the pattern of the isotherms. The isotherms did not spread as far across the channel as the experimental data. This was apparently due to a smaller spread of the jet shown in Figure 19 due to the grid spacing.

FIGURE 21
Surface Isotherm Prediction

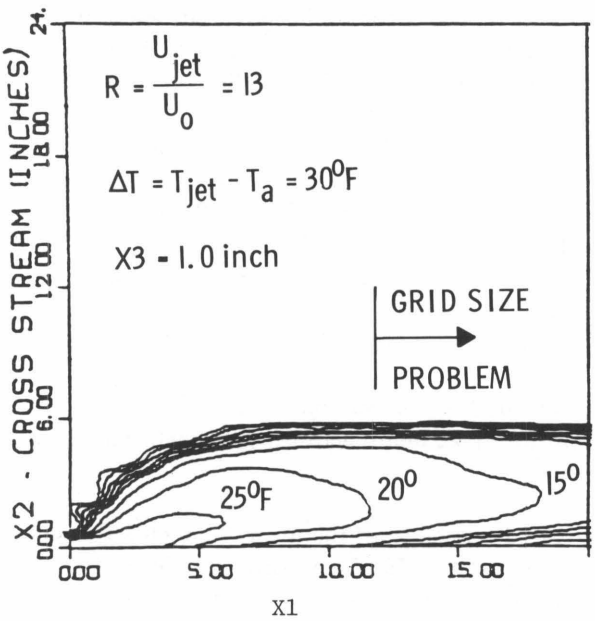

COMPARATIVE STUDY OF THE EFFECTS OF DISCHARGE GEOMETRY ON THE THERMAL MIXING ZONE

I. Flow Channel

The same basic channel used for the experiments described in the earlier sections was used here.

II. Injection Systems

Three more types of injector geometry were tested—one multiple port diffuser and two single jet discharges. All had the same total total exit area. The multiple port diffuser had a single row of 47 ports (0.070 inch diameter, 0.5 inch center-to-center) drilled vertically into the channel floor, going across the width of the channel. The diffuser ports were individually connected to a 3.5 inch diameter manifold, located underneath the channel, by 6 inch lengths of 0.25 inch plastic tubing. The single jet injectors directed the discharge perpendicular to the main flow by means of circular outlets (0.5 inch diameter) in the sidewall. One had the outlet centerline on the water surface (surface jet), and the other rested at the bottom of the channel (submerged jet). The single-jet discharge results described in the previous Results section also can be considered here for comparative purposes. For dyed injectant tests to permit flow visualization, the jet fluid came from a 14-gallon insulated tank, closed and pressurized with an air supply and a regulator valve. Just prior to the dye experiments, the tank was filled with hot water dyed with a mixture of red and blue food coloring. During the remainder of the tests, the jet fluid was tapped from the main feed line on the positive pressure side of the pump, and run through a heat exchanger to gain 30° F in temperature. The heat exchanger is stainless steel (9 feet long by 4.5 inches diameter), utilizing counter-current flow through multiple parallel tubes.

During all the tests the jet fluid passed through a needle valve, a flowmeter, and a ball valve, in that order. From the ball valve, the jet fluid entered either the jet injectors or the diffuser manifold. All lines transporting the jet fluid were of plastic in order to minimize heat losses.

III. Test Conditions

All tests were run with a 1.0-inch depth at the injection station. Injectant to freestream temperature differences of 0, 15 and 30° F were considered. Freestream velocities of 0.23, 0.32, 0.43 and 0.61 inch per second were tested while holding the injectant (area averaged) velocity at a nominal value of 3.4 inches per second. An application of Murphy's Perverse Law produced a jet velocity of 3.0 inches per second for the parallel jet tests. In any event, this group of conditions covered a wide range of practical interest in terms of injectant to freestream velocity and mass flow ratios.

FIGURE 22

Flow Visualization for Dyed Submerged Jet,
$\Delta T = 16.7^\circ$ C, $U_{jet}/U_{main} = 14.8$

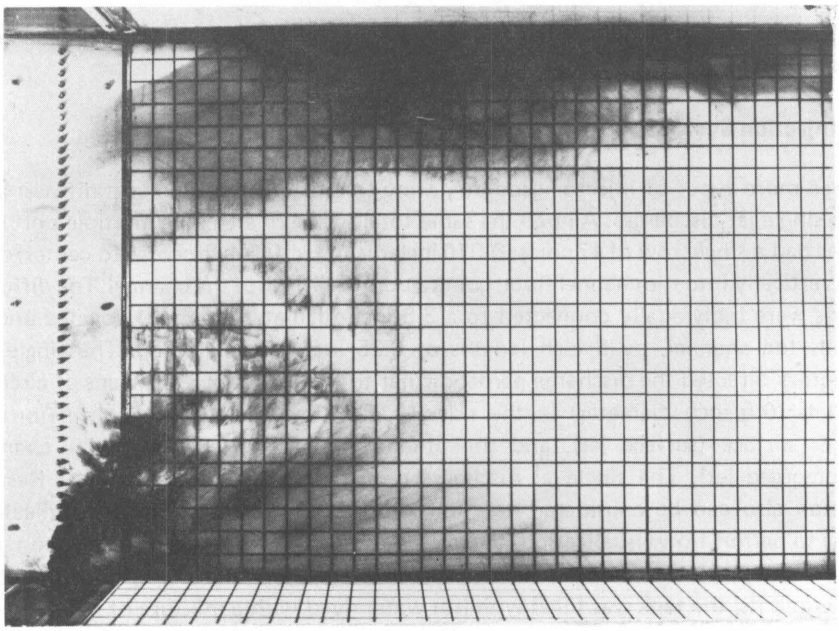

IV. Results

Complete detailed results for all of the conditions tested are presented in Payne and Schetz [1974] and Cannon and Schetz [1975]. Due to space limitations, we can present only isolated examples of particular interest here. In order to orient the reader, some flow visualization results pertaining to recirculation zones and "hot spots" are shown first and then some detailed surface temperature distributions will be given.

A. Recirculation Zones and Hot Spots

For the purpose of illustrating the different ways massive recirculation zones can occur, we have selected first an example from the parallel jet injection studies described in the previous Results section. Recall that for unheated jet injection and for many combinations of temperature difference and jet and freestream velocities, the outer boundary of the mixing zone simply spreads laterally across the channel as one proceeds downstream. For certain combinations of temperature difference and velocity ratio, however, the whole flowfield is altered and large recirculation zones appear (Figure 11).

The occurrence of a hot spot by a completely different means can be illustrated by examining one of the submerged jet cases shown in Figure 22. It was clearly evident during the experiment that the heated fluid rose to the surface and floated at the top while its later momentum carried it across stream. A continuous sheet of buoyant fluid was moving toward the boundary. When it reached there, it was forced (by conservation of mass and momentum) to turn downward or travel along the boundary. Thus, an accumulation of this dyed fluid, at the boundary, gives a darker appearance in the photograph. It is evident that a part of the dyed fluid has migrated upstream, along that boundary, even beyond the initial station of the discharging jet. Two conditions probably allow this. First, the fluid mass flowing toward the boundary must eventually lose its velocity in the spanwise direction, and because of the flow continuum in that direction, must assume some axial component of velocity, be it upstream or downstream. Second, the relatively low streamflow in this case may produce sufficiently low velocity near the wall, so that the buoyant flow may propagate upstream.

B. Surface Temperature Distribution

Our studies included detailed temperature distributions in the spanwise, vertical and axial directions and complete results are given in Payne and Schetz [1974] and Cannon and Schetz [1975]. Here, we will show representative surface isotherm patterns for the various injectors. Surface isotherms are of particular interest, since it is these which are commonly regulated by law and since they reflect the rapidity at which heat is transferred to the atmosphere and thus out of the waterway. The isotherms were generated from the raw data with an IBM 370 computer, using a modified three-dimensional spline interpolating function, and graphed on a Calcomp plotter.

The case selected for direct comparison was that for which the free stream velocity was 0.23 inch per second for all injectors. The results for the parallel single jet injector are shown in Figure 23a. It is evident that the higher valued isotherms terminate quickly as a result of the mixing due to entrainment. The fact that the jet rises and the free stream fluid has direct access to the hotter portion of the jet (near the wall) enhances this effect. This region, then, cools much more rapidly than if all entrained fluid had to reach the wall by turbulent transport across the entire width of the jet. Even with an increased interface area, the entrained fluid still requires a finite length of time to mix with the jet fluid and make its presence known throughout the jet.

In Figure 23b, we show the corresponding results for the surface jet injector. In this case, warmer fluid penetrates much more rapidly across the channel. However, the rate of downstream decay of the temperature difference is much more rapid. Also, the temperature patterns themselves are more irregular.

Next, Figure 23c displays the results for the submerged jet injector. The temperature

FIGURE 23

Surface Isotherm Patterns

$\Delta T = 16.7^{\circ}$ C

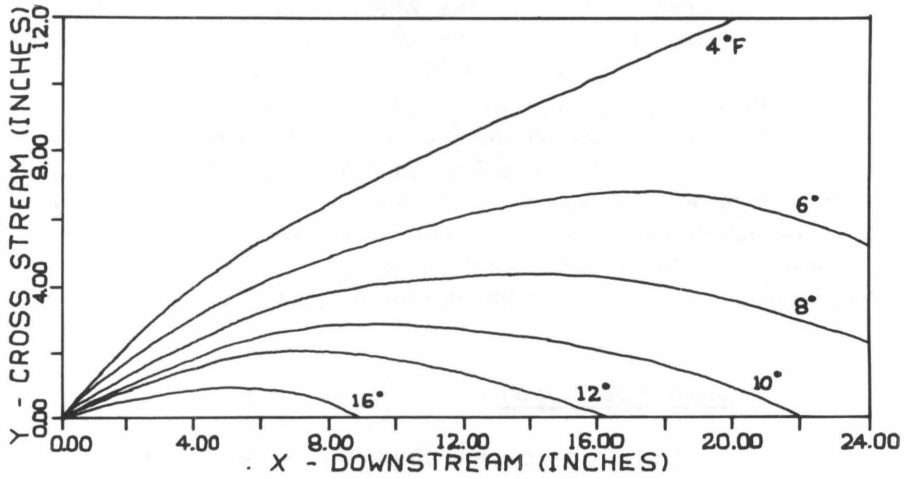

a. Parallel Jet Injection $U_{jet}/U_{main} = 13$

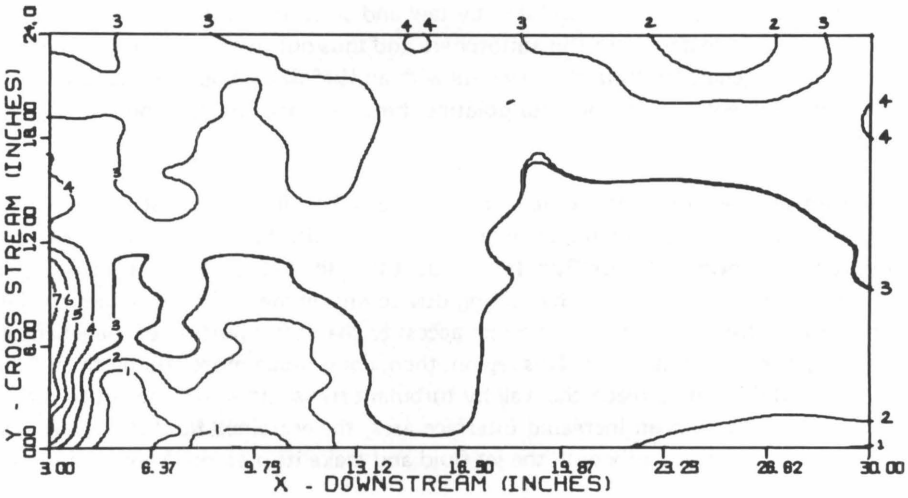

b. Surface Jet Injector $U_{jet}/U_{main} = 14.8$

Figure 23
continued

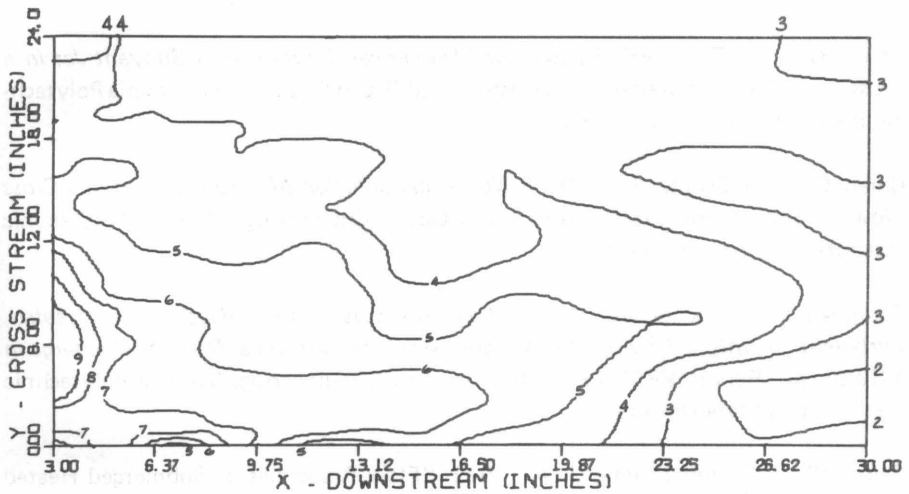

(c) Submerged Jet Injector U_{jet}/U_{main} = 14.8

differences all across the surface are larger than that for the surface jet at the same conditions. This is a result of the reduced heat transfer from the jet to the atmosphere in the vicinity of the discharge since it was below the surface in that region.

The results for the multi-port diffuser are not displayed graphically here in order to conserve space and also because they showed fewer distinctive features. The surface temperatures were much more uniform than any of the previous cases and the values were lower. This results from the greatly increased rate of mixing with the main flow. For comparison with the other results, it is noteworthy that the maximum ΔT had reduced to less than 4° F by the X = 10 inches station.

REFERENCES

Abramovich, G. N., 1962. *Turbulent Jets.* MIT Press, Cambridge.

Chien, C. J., 1973. *User's Manual for "Numerical Solution of a Buoyant Jet in a Cross Flow."* Report Aero-500. Aerospace and Ocean Engineering. Virginia Polytechnic Institute and State University.

Chien, C. J. and Schetz, J. A., 1973. *Numerical Solution of a Buoyant Jet in a Cross Flow.* Report Aero-001, Aerospace and Ocean Engineering. Virginia Polytechnic Institute and State University.

Campbell, J. F. and Schetz, J. A., 1972. *Analysis of the Injection of a Heated, Turbulent Jet into a Moving Mainstream, with Emphasis on a Thermal Discharge in a Waterway.* Report VPI-E-72-24.Department of Engineering. Virginia Polytechnic Institute and State University.

Campbell, J. F. and Schetz, J. A., 1973. "Flow Properties of Submerged Heated Effluents in a Waterway." *AIAA Journal.* Vol.11, No. 2 pp. 223-230.

Cannon, S. and Schetz, J. A. 1975. *Comparative Study of Discharge Designs in Waterways.* VPI-Aero-033. Aerospace and Ocean Engineering. Virginia Polytechnic Institute and State University.

Eckert, E.R. G. and Drake, R. M., Jr., 1959. *Heat and Mass Transfer.* 2nd ed. McGraw-Hill.

Goldstein, R. J., and Kreid, D. K., 1967. "Measurement of Laminar Flow Development in a Square Duct Using a Laser-Doppler Flowmeter." *Journal of Applied Mechanics.*

Goseman, A. D.; Pun, W. M.; Runchal, A. K.; Spalding, D. B., and Wolfshtein, M., 1969. *Heat and Mass Transfer in Recirculating Flows,* Academic Press, Inc., Ltd.

Harlow, F. H., 1973. *Turbulence Transport Modeling,* AIAA Selected Reprint Series. Vol. XIV.

Launder, B. E. and Spalding, D. B., 1972. *Lectures in Mathematical Models of Turbulence.* Academic Press, New York.

Markham, D. M. 1975. *Numerical Solutions to the Three-Dimensional Navier-Stokes Equations for a Turbulent, Heated Jet into a Shallow Channel.* Master's thesis. Virginia Polytechnic Institute and State University.

Payne, J. A., and Schetz, J. A., 1974. *An Experimental Comparison of Thermal Discharges to a Waterway by a Single Jet and a Multiple Port Diffuser.* VPI-E-74-21. Department of Engineering. Virginia Polytechnic Institute and State University. Available through National Technical Information Service.

Sill, B. L. and Schetz, J. A., 1973. *Studies of a Heated Turbulent Jet in a Shallow, Bounded Waterway.* Report Aero-005. Aerospace and Ocean Engineering, Virginia Polytechnic Institute and State University.

Thompson, J. F., 1971. *Two Approaches to the Three-Dimensional Jet-in-cross-wind Problem: A Vortex Lattice Model and a Numerical Solution of the Navier-Stokes Equations.* Ph. D. thesis. Georgia Institute of Technology.

VIRGINIA WATER RESOURCES RESEARCH CENTER
BLACKSBURG, VIRGINIA 24061